Compact modeling of gate engineered triple material gate (TMG) AlInSb/InSb high electron mobility transistors

S. THEODORE CHANDRA*, N. B. BALAMURUGAN, G. LAKSHMI PRIYA, V. MURALIDHARAN, D. S. SUGIRTHA RUBA RANI
National Instruments Electronics Laboratory, Department of ECE, Thiagarajar College of Engineering, Madurai, Tamilnadu - 625015, India.

A two dimensional analytical model is developed for the Triple Material Gate (TMG) AlInSb/InSb HEMT devices by solving the 2D Poisson equation. We use three gate materials of different work functions in this structure. The analytical model is obtained by solving the Poisson equation using parabolic approximation method to extract the parameters like channel potential, electric field distribution and threshold voltage. Due to the step in the surface potential profile, the drain current is screened from the source side, thereby suppressing the short channel effects in this structure. By considering the variation of gate source voltage, channel length under different metal regions and temperature, the working of the HEMT device is analyzed. The uniform electric field along the channel which is created by the small difference in the voltage improves the carrier transport efficiency. This difference in voltage is due to different work functions of the three materials used in the gate region. The results of the analytical model are compared with simulation results obtained from Sentarus TCAD and a good agreement between them is achieved.

(Received October 15, 2014; accepted January 21, 2015)

Keywords: High Electron Mobility Transistor (HEMT), Gate engineering, Quantum well device, Poisson's equation, Channel potential, Electric field.

1. Introduction

AlInSb/InSb high electron mobility transistors (HEMTs) has vital role in high current, high voltage, high power and high frequency operations [1-3]. The materials used in this HEMT device possess the advantage of high current drivability, thermal stability and high breakdown fields. Indium Antimonide is a dark grey material with zincblende crystal structure has the advantage of lowest band gap 0.1eV at room temperature and 0.23eV at 80 K and highest lattice constant 0.64 nm than any other quantum well formed of III and V group material system. The largest ambient-temperature electron mobility of undoped InSb quantum well is found to be approximately as high as 78, 000 cm^2/V-s than any other material. Hence quantum well formed by sandwiching layers of AlInSb/InSb help to construct fastest transistors. It is a trend in the compound semiconductor industry to continuously develop devices which are extremely small, fast and consumes less power [5, 6]. One of the most effective ways of improving the performance of HEMT devices is to reduce their size [6]. However, the scaling of HEMT devices has its own limits. Scaling beyond the limit reduces the carrier transport efficiency and introduces short channel effects. [7, 8].

To overcome these disadvantages various novel architectures like Double gate, Dual material gate, Dual material Double gate, Dual channel are proposed. But these methods do not improve the carrier transport efficiency. Dual channel structure was first proposed in 1984, which offers larger output current and higher transconductance. The high electron affinity in the InGaAs channel may induce impact ionization of charge carriers under high electric field, which leads to high leakage current and this is a major concern in the dual channel structure. Split-Gate (SG) FET [10, 11] increases the carrier transport efficiency, but the inherent fringing capacitance between the two very closely separated gates affects the high speed performance of the device. But these approaches have not shown any improvement in the carrier transport efficiency and SCEs suppression simultaneously. However our proposed TMG HEMT Structure overcomes these issues. Due to the step in the surface potential profile, the drain current is screened from the source side, thereby suppressing the short channel effects in this structure. The uniform electric field along the channel which is created by the small difference in the voltage due to three different gate material regions improves the carrier transport efficiency.

In this work a two dimensional analytical model is developed for the Triple Material Gate (TMG) AlInSb/InSb HEMT device by solving the 2D Poisson equation using the parabolic approximation method. Parameters like surface potential, electric field distribution and threshold voltage are calculated in order to estimate the device performance. The rest of the paper is organized as follows: Section 2 presents the schematic device structure of AlInSb/InSb HEMT device. Section 3 deals with our model formulation for TMG AlInSb/InSb HEMT device which includes analysis of channel potential. In section 4 the electric field is derived. Results and discussion is presented in section 5, where

analytical model results are compared with TCAD simulation results. Conclusion is given in section 6.

2. Device structure of AlInSb/InSb HEMT

In the proposed TMG HEMT structure three materials of different work functions are used. Figure 1 shows the schematic view of the TMG AlInSb/InSb HEMT with three gate materials of different work functions φ_{M1}, φ_{M2} and φ_{M3}. The gate materials are φ_{M1} = 4.8 eV (Au), φ_{M2} = 4.4 eV (Ti) and φ_{M3} = 4.1 eV (Al), which are chosen in such a way that $\varphi_{M1} > \varphi_{M2} > \varphi_{M3}$. As a result, the threshold voltage will be in the order of $V_{th1} > V_{th2} > Vth_3$. The gate region M_1 near the source side is the first screen gate region, the gate region M_2 in the middle is the control gate region and the gate region M_3 near the drain side is the second screen gate region.

Basically, the structure consists of a semi-insulating GaAs substrate, on which is first grown a undoped InSb layer; then an delta doped AlInSb layer followed by the spacer, then a doped AlInSb layer and the capacitive layer. The capacitive layer is highly doped in order to minimize the contact resistance of the source and drain contacts. The transistor is finally realized by depositing three different gate materials to form a Schottky barrier and serve as the gate, and by providing two ohmic contacts to serve as the source and the drain. The transistors may be operated in two modes, normally-on mode and normally off mode. This is determined by the thickness of the AlInSb layers. When these layers are thick enough, charge is supplied by the layer to fill up the surface states at the interface between it and the gate metal and also to the InSb layer for the alignment of the Fermi levels. The transistor is normally-on. If, on the other hand, the barrier layer is made thin, then the charge available in the layer is not enough to cause alignment) of the Fermi levels and the InSb layer is required to supply additional charge. The layer being depleted, the transistor is normally-off. Both these transistors are required for different functional circuits.

In high-electron-mobility-transistors (HEMTs) the heterojunction between two semiconducting materials confine electrons to a triangular quantum well and form two-dimensional electron gas (2DEG). The two-dimensional electron gas is nothing but electrons which are free to move in two dimensions, but tightly confined in the third dimension. Thus the electrons appear to be a two dimensional sheet of charge. The mobility of electrons confined to the heterojunction of HEMTs is higher than that of MOSFETs. Here the junction between the n-doped AlInSb and undoped InSb layer is the source of 2DEG. The model which includes the polarization effect would be valuable but it is beyond scope of this work. However, the model in its current form would be useful for predicting the performance enhancement of the DMG HEMT and the device structure optimization as the currents in the sub-threshold regime are small.

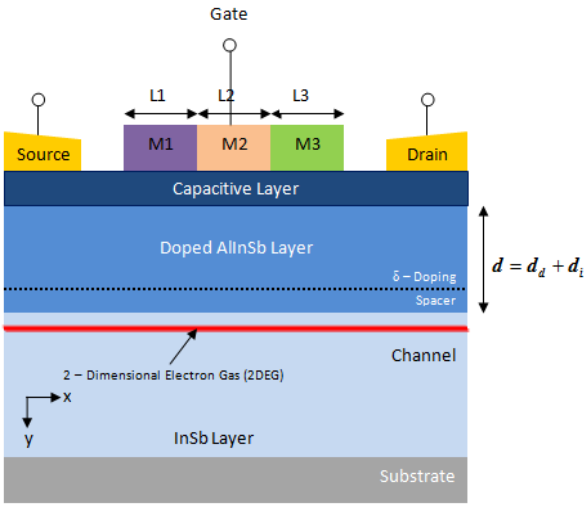

Fig.1. Schematic view of TMG AlInSb/InSb HEMT. L_1, L_2, and L_3 are the lengths of gate materials M_1, M_2 and M_3

3. Model formulation

The proposed model analyses the channel potential, electric field distribution and threshold voltage which are obtained by solving the 2D Poisson equation using parabolic approximation method. The solution to Poisson equation can be obtained by different methods such as Superposition method, Fourier series expansion, Green function, Newton Raphson method, Parabolic approximation method [12, 13]. Since the other methods are slightly difficult and complex, we use the parabolic approximation method in order to make the model simple and accurate. The channel region is divided into three parts, since three materials have been used in the gate region. The source and the drain regions are uniformly doped. The 2-D potential distribution (x, y) can be obtained by solving the 2-D Poisson's equation which is rewritten from the book authored by Jean-Pierre Colinge [14], and is given by

$$\frac{d^2\phi(x,y)}{dx^2}+\frac{d^2\phi(x,y)}{dy^2}=-\frac{qN_d}{\varepsilon_a} \quad \text{for } 0\le x\le L \tag{1}$$

where N_d is the doping density of the AlInSb layer, q is the electric charge, ε_a is the dielectric constant and $L= L_1+L_2+L_3$ is the effective channel length.

$$\phi(x,y)=\phi_l(x)+C_1(x)(y-d)+C_2(x)(y-d)^2 \tag{2}$$

ϕ_l is the channel potential, $d = d_d + d_i$ is the thickness of the AlInSb layer with d_s as the thickness of the doped AlInSb and d_i as the thickness of the spacer layer. $C_1(x)$ and $C_2(x)$ are arbitrary coefficients. Equation (2) must satisfy the boundary conditions.

In the TMG HEMT structure, the gate has been divided into three parts; hence the potential under the different gate region is given as follows,

The potential under the gate region M_1 near the source side (first screen gate region) is,

$$\phi_1(x,y) = \phi_{l1}(x) + C_{11}(x)(y-d) + C_{21}(x)(y-d)^2 \quad 0 \le x \le L_1 \tag{3}$$

The potential under the gate region M_2 in the middle (control gate region) is,

$$\phi_2(x,y) = \phi_{l2}(x) + C_{12}(x)(y-d) + C_{22}(x)(y-d)^2 \quad L_1 \le x \le L_1 + L_2 \tag{4}$$

The potential under the gate region M_3 near the drain side (second screen gate region) is,

$$\phi_3(x,y) = \phi_{l3}(x) + C_{13}(x)(y-d) + C_{23}(x)(y-d)^2 \quad L_1 + L_2 \le x \le L_1 + L_2 + L_3 \tag{5}$$

The Poisson's equation is solved separately under the three gate regions using the following boundary conditions:

1. Channel Potential at the interface of the three dissimilar metals is continuous [17-20]

$$\phi_1(L_1, d) = \phi_2(L_1, d) \quad \text{at} \quad x = L_1 \tag{6}$$

$$\phi_2(L_1 + L_2, d) = \phi_3(L_1 + L_2, d) \tag{7}$$

2. Electric field at the interface of the three dissimilar metals is continuous [17-20]

$$\frac{d\phi_1(x,y)}{dx} = \frac{d\phi_2(x,y)}{dx} \quad x = L_1 \tag{8}$$

$$\frac{d\phi_2(x,y)}{dx} = \frac{d\phi_3(x,y)}{dx} \quad x = L_1 + L_2 \tag{9}$$

3. $$\phi_1(x,0) = V_{g1} \tag{10}$$

$$\phi_2(x,0) = V_{g2} \tag{11}$$

$$\phi_3(x,0) = V_{g3} \tag{12}$$

where $V_{g1} = V_{gs} - V_{FB1}$, $V_{g2} = V_{gs} - V_{FB2}$, $V_{g3} = V_{gs} - V_{FB3}$ and V_{gs} is the gate to source voltage.

4. $$\frac{d\phi_1(x,y)}{dy}\bigg|_{y=d} = -E_{\text{int}1} \tag{13}$$

$$\frac{d\phi_2(x,y)}{dy}\bigg|_{y=d} = -E_{\text{int}2} \tag{14}$$

$$\frac{d\phi_3(x,y)}{dy}\bigg|_{y=d} = -E_{\text{int}3} \tag{15}$$

where $E_{\text{int}1}, E_{\text{int}2}, E_{\text{int}3}$ are the fields at the hetero interface under M_1, M_2 and M_3 respectively.

5. The potential at the source end is

$$\phi_1(0,d) = V_{bi} \tag{16}$$

where V_{bi} is the built in voltage.

6. The potential at the drain end is

$$\phi_2(L_1 + L_2 + L_3, d) = V_{bi} + V_{ds} = \phi_{l2}(L_1 + L_2 + L_3) \tag{17}$$

where V_{ds} is the drain to source voltage of the device.

The constants in (3), (4) and (5) can be found from boundary conditions (6)–(17) and on substituting their values in (3), (4) and (5), we get

$$\phi_j(x,y) = \phi_{lj}(x) - E_{\text{int}}(y-d) + \left[\frac{V_{gj} - \phi_{lj}(x)}{d^2} - \frac{E_{\text{int}j}}{d}\right](y-d)^2 \tag{18}$$

where j = 1,2,3 for regions under M_1, M_2 and M_3 respectively.

The channel potential $\phi_{lj}(x)$ is obtained by substituting (18) in (1). On Substitution, we get

$$\frac{d^2\phi_{lj}(x,y)}{dx^2} + \frac{V_{gj} - \phi_{lj}(x)}{\lambda^2} = -\frac{qN_d}{\varepsilon_a} + \frac{2E_{\text{int}j}}{d} \tag{19}$$

where λ is the characteristic length and it is given by

$$\lambda = \sqrt{\frac{d^2}{2}} \tag{20}$$

Introducing a new variable

$$\eta_j(x) = \phi_{lj}(x) - V_{gj} - \left[\frac{qN_d}{\varepsilon_a} - \frac{2E_{\text{int}\,j}}{d}\right]\lambda^2 \tag{21}$$

and substituting (21) in (19), we get

$$\frac{d^2\phi\,(x,y)}{dx^2} + \frac{\eta_j(x)}{\lambda^2} = 0 \tag{22}$$

Using (21), $\eta_j(x=0) = \eta_{11}$, $\eta_j(x = L_1 + L_2) = \eta_{22}$, $\eta_j(x = L_1 + L_2 + L_3) = \eta_{33}$ and the boundary conditions (5) and (6) we get

$$\eta_{11} = V_{bi} - V_{g1} - \left[\frac{qN_d}{\varepsilon_a} - \frac{2E_{\text{int1}}}{d}\right]\lambda^2 \tag{23}$$

$$\eta_{22} = (\eta_{11} + V_{ds}) - (V_{fb1} - V_{fb2}) - (b_2 - b_1)^2 \tag{24}$$

$$\eta_{33} = (\eta_{11} + V_{ds}) - (V_{fb1} + V_{fb2} - V_{fb3}) - (b_2 + b_1 - b_3)^2 \tag{25}$$

where $b_1 = \frac{qN_d}{\varepsilon_a} - \frac{2E_{\text{int}\,1}}{d}$, $b_2 = \frac{qN_d}{\varepsilon_a} - \frac{2E_{\text{int}\,2}}{d}$ and $b_3 = \frac{qN_d}{\varepsilon_a} - \frac{2E_{\text{int}\,3}}{d}$

Solving (22) for $\eta_{j(x)}$ and substituting in (21), we obtain the channel potential $\phi_{lj}(x)$ as

$$\varphi_{l1}(x) = \frac{\eta_{11}\sinh\left[\frac{L_1 - x}{\lambda}\right] + \eta_{12}\sinh\left[\frac{x}{\lambda}\right]}{\sinh\left[\frac{L_1}{\lambda}\right]} + V_{g1} + \left[\frac{qN_d}{\varepsilon_a} - \frac{2E_{\text{int1}}}{d}\right]\lambda^2 \tag{26}$$

$$\varphi_{l2}(x) = \frac{\eta_{22}\sinh\left[\frac{x - L_2}{\lambda}\right] + \eta_{21}\sinh\left[\frac{L_1 + L_2 - x}{\lambda}\right] + \eta_{23}\sinh\left[\frac{L_1 + L_2 + L_3 - x}{\lambda}\right]}{\sinh\left[\frac{L_2}{\lambda}\right]} + V_{g2} + b_2\lambda^2 \tag{27}$$

$$\varphi_{l3}(x) = \frac{\eta_{33}\sinh\left[\frac{x - L_3}{\lambda}\right] + \eta_{32}\sinh\left[\frac{L_1 + L_2 + L_3 - x}{\lambda}\right]}{\sinh\left[\frac{L_3}{\lambda}\right]} + V_{g3} + b_3\lambda^2 \tag{28}$$

$$\text{Let } \alpha_i = \frac{L_i}{\lambda}, \text{ where i = 1,2,3} \tag{29}$$

Using boundary conditions (6) to (8), and (23) to (29), we obtain the values of $\eta_{12,}, \eta_{21}, \eta_{32}, \eta_{23}, \eta_{31}, \eta_{13}$ as

$$\eta_{12} = \frac{\eta_{11}\sinh\alpha_2 + \eta_{22}\sinh\alpha_1 + (V_{g2} - V_{g1})\sinh\alpha_1\cosh\alpha_2 + (b_2 - b_1)^2\sinh\alpha_1\cosh\alpha_2}{\cosh\alpha_1\sinh\alpha_2 + \cosh\alpha_2\sinh\alpha_1} \tag{30}$$

$$\eta_{21} = \frac{\eta_{22}\sinh\alpha_1 + \eta_{11}\sinh\alpha_2 + (V_{g1} - V_{g2})\sinh\alpha_2\cosh\alpha_1 + (b_1 - b_2)^2\sinh\alpha_2\cosh\alpha_1}{\cosh\alpha_2\sinh\alpha_1 + \cosh\alpha_1\sinh\alpha_2} \tag{31}$$

$$\eta_{32} = \frac{\eta_{33}\sinh\alpha_2 + \eta_{22}\sinh\alpha_3 + (V_{g2} - V_{g3})\sinh\alpha_3\cosh\alpha_2 + (b_2 - b_3)^2\sinh\alpha_3\cosh\alpha_2}{\cosh\alpha_3\sinh\alpha_2 + \cosh\alpha_2\sinh\alpha_3} \tag{32}$$

$$\eta_{23} = \frac{\eta_{22}\sinh\alpha_3 + \eta_{11}\sinh\alpha_2 + (V_{g3} - V_{g2})\sinh\alpha_2\cosh\alpha_3 + (b_3 - b_2)^2\sinh\alpha_2\cosh\alpha_3}{\cosh\alpha_2\sinh\alpha_3 + \cosh\alpha_3\sinh\alpha_2} \tag{33}$$

$$\eta_{31} = \frac{\eta_{33}\sinh\alpha_1 + \eta_{11}\sinh\alpha_3 + (V_{g1} - V_{g3})\sinh\alpha_3\cosh\alpha_1 + (b_1 - b_3)^2\sinh\alpha_3\cosh\alpha_1}{\cosh\alpha_3\sinh\alpha_1 + \cosh\alpha_1\sinh\alpha_3} \tag{34}$$

$$\eta_{13}=\frac{\eta_{11}\sinh\alpha_3+\eta_{33}\sinh\alpha_1+(V_{g3}-V_{g1})\sinh\alpha_1\cosh\alpha_3+(b_3-b_1)^2\sinh\alpha_1\cosh\alpha_3}{\cosh\alpha_1\sinh\alpha_3+\cosh\alpha_3\sinh\alpha_1} \tag{35}$$

4. Analysis of Electric Field

The surface electric field component along the channel in the x-direction is an important parameter as the electron transport velocity through the channel is directly related to the electric field along the channel, whose x-component under M_1 is given by,

$$E_1(x)=\frac{d}{dx}\varphi_1(x,y)\Big|_{y=d}=\frac{d\phi_{l1}(x)}{dx}$$

$$E_1(x)=\frac{\eta_{11}\cosh\left[\frac{L_1-x}{\lambda}\right]\left[-\frac{1}{\lambda}\right]+\eta_{12}\cosh\left[\frac{x}{\lambda}\right]\left[\frac{1}{\lambda}\right]}{\sinh\alpha_1} \tag{36}$$

and x-component under M_2 is

$$E_2(x)=\frac{d}{dx}\varphi_2(x,y)\Big|_{y=d}=\frac{d\phi_{l2}(x)}{dx}$$

$$E_2(x)=\frac{\eta_{22}\cosh\left[\frac{x-L_2}{\lambda}\right]\left[\frac{1}{\lambda}\right]+\eta_{21}\cosh\left[\frac{L_1+L_2-x}{\lambda}\right]\left[-\frac{1}{\lambda}\right]+\eta_{23}\cosh\left[\frac{L_1+L_2+L_3-x}{\lambda}\right]\left[-\frac{1}{\lambda}\right]}{\sinh\alpha_2} \tag{37}$$

and x-component under M_3 is

$$E_3(x)=\frac{d}{dx}\varphi_3(x,y)\Big|_{y=d}=\frac{d\phi_{l3}(x)}{dx}$$

$$E_3(x)=\frac{\eta_{33}\cosh\left[\frac{x-L_3}{\lambda}\right]\left[\frac{1}{\lambda}\right]+\eta_{32}\sinh\left[\frac{L_1+L_2+L_3-x}{\lambda}\right]\left[-\frac{1}{\lambda}\right]}{\sinh\alpha_3} \tag{38}$$

5. Results and Discussion

The proposed analytical model for TMG AlInSb/InSb HEMT has been simulated using MATLAB simulator and validated using TCAD device simulator [15]. The electrical characteristics of semiconductor devices is simulated using device simulation tools, as a response to external electrical, thermal or optical boundary conditions imposed on the structure. The Sentaurus Structure Editor tool is used to create the input device structure. Depending on the device under analysis Sentaurus Device includes carrier transport models like drift diffusion model which accounts for isothermal simulation and hydrodynamic model which accounts for temperature effects.

Fig.2 shows the variation of channel potential with the normalized channel position for TMG AlInSb/InSb. It can be inferred that when compared with DMG, TMG has greater channel potential and this leads to greater ON current. Fig.3. depicts the plot of channel potential variation of TMG AlInSb/InSb HEMT for different V_{ds}. It is observed that due to the difference in work functions of three metal regions, the drain side is screened from the source side thereby reducing short channel effect, it is observed that as distance from channel increases, the channel potential also increases.

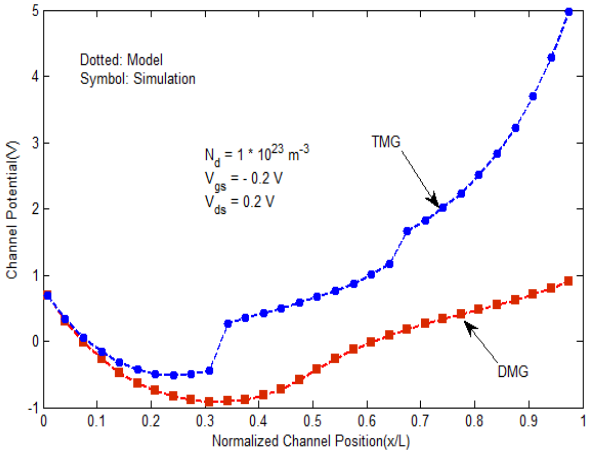

Fig.2.Variation of channel potential with the normalized channel position for TMG AlInSb/InSb HEMT

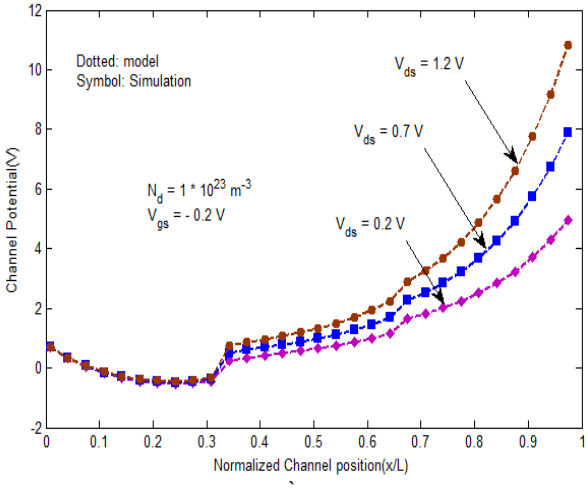

Fig.3.Variation of channel potential of TMG AlInSb/InSb HEMT for different V_{ds}

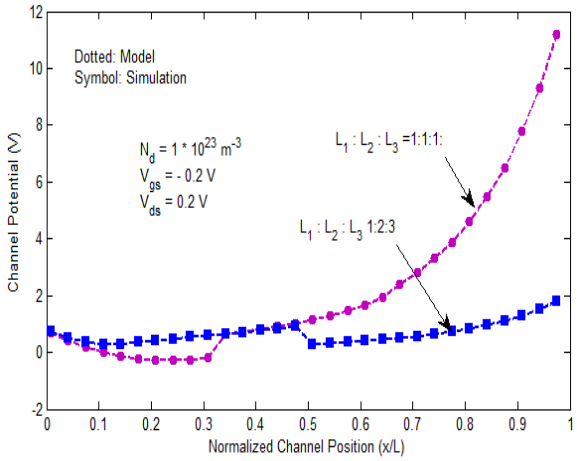

Fig.4.Variation of channel potential of TMG AlInSb/InSb HEMT for different gate material Length

Fig.5. shows the variations of channel potential along the channel position for different values of temperature. It is observed that increase in temperature leads to decrease in surface potential in the channel. This clearly shows that as temperature decreases to cryogenic temperature, there is a greater channel potential and leads to increased performance. Hence, HEMT can be used for Cryogenic purposes.

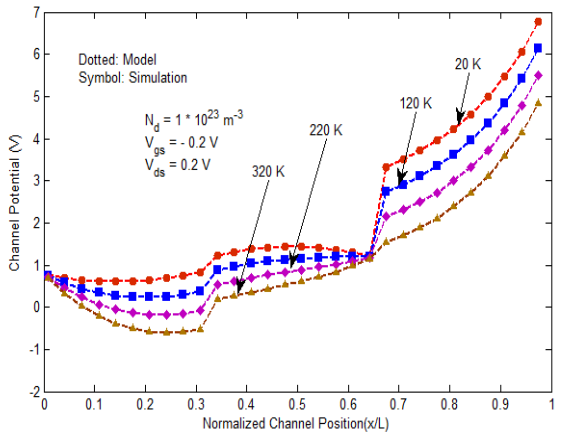

Fig.5. Variation of channel potential of TMG AlInSb/InSb HEMT for different Temperature

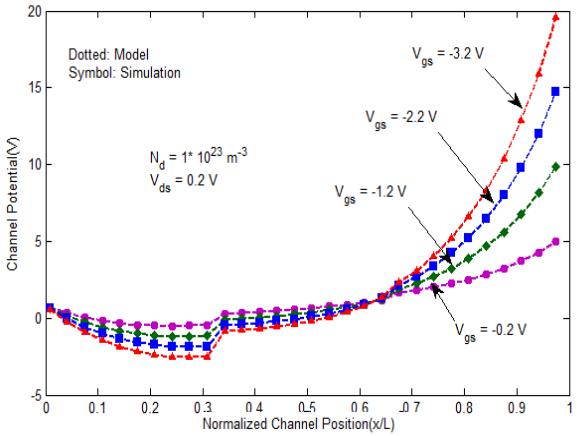

Fig.6.Variation of channel potential of TMG AlInSb/InSb HEMT for different V_{gs}.

Fig.6. shows the plot of variation of channel potential for different values of gate to source voltages. While we plot for various V_{gs}, it is observed that for more negative V_{gs}, there is an increase in the channel potential. The TCAD simulations are compared with the analytical results and a good match between them is observed.

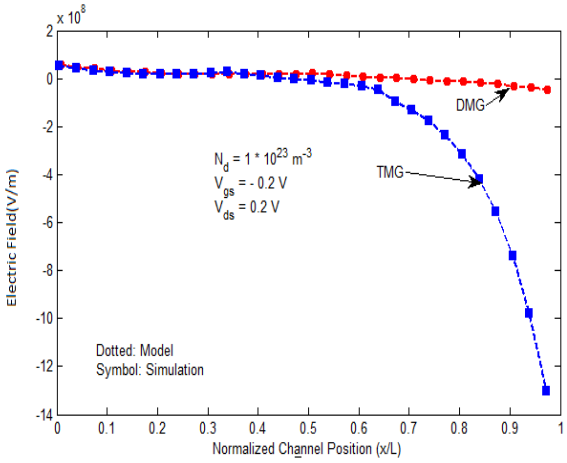

Fig.7.Variation of Electric Field of TMG AlInSb/InSb HEMT.

Fig.7. shows the electric field variation along the channel position for TMG and DMG HEMT. It is inferred that the electric field at the drain end is considerably low for TMG HEMT than DMG HEMT. This is due to the screening effect, where excess drain voltage is absorbed by the M_3 region. Hence M_1 region is screened from the drain potential variations, which reduces the peak electric field towards the drain end. This ensures reduced short channel effects and increased lifetime of the device.

6. Conclusions

The effectiveness of the triple material gate concept to the AlInSb/InSb HEMTs has been examined for the first time by developing a 2-D analytical model. Expressions for the channel potential, electric field, and sub-threshold drain current have been obtained, proving the superiority of TMG AlInSb/InSb HEMT in suppressing the SCEs over the conventional DMG structure. The results obtained from the model agree well with the simulation results. It is apparent from the results that the TMG architecture exhibits improved gate controllability over the channel. Results also emphasize that the device optimization in terms of the metal gate length ratios, work function differences, and barrier layer thicknesses, leads to improvement in the device performance. Thus, the introduction of the TMG HEMT structure enhance the gate transport efficiency but also suppress the short channel effects including darin induced barrier lowering and hot electron effect. It also shows the potential for many future applications where high performance HEMTs, with gate lengths down to sub-100 nm, are required.

Acknowledgement

This work was supported by the Council of Scientific & Industrial Research (CSIR), India under the Senior Research Fellowship scheme (Sanction Letter No: 08/237(0005)/2012-EMR-I).

References

[1] Nicolas Faralli, Himanshu Markandeya, Julien Branlard, Marco Saraniti, Stephen M. Goodnick, David K. Ferry, Journal of Computational Electronics, **5(**4), 483 (2006).
[2] C. Liu, Y. Li, Y. Zeng, Engineering, **2(**8), 617 (2010).
[3] B. R. Bennett, R. Magno, J. Brad Boos, Walter Kruppa, Mario G. Ancona, Solid-State Electronics, **49(**12), 1875 (2005).
[4] S. J. Lee, C.R. Crowell, C. P. Lee, Electron Devices Meeting, **29**, 103 (1983).
[5] R. M. Biefeld, Materials Science and Engineering R, **36(**4), 105 (2002).
[6] L.D. Nguyen, L.E. Larson, U.K. Mishra, Proceedings of IEEE, **80**(4), 494 (1992).
[7] G. Tuttle, H. Kroemer, J.H. English, Journal of Applied Physics, **65**(12), 5239(1989).
[8] Rashmi, A. Agrawal, S. Sen, S. Haldar, R.S. Gupta, Microwave Optical Technology Letters **29**, 117 (2001).
[9] S. Kumar, A. Agrawal, S. Kabra, M. Gupta, R.S. Gupta, Microelectronics Journal, **37**, 1339 (2006).
[10] S. P. Kumar, A. Agrawal, R. Chaujar, M. Gupta, R.S.Gupta, Superlattices and Microstructures, **44**, 37 (2008).
[11] W. Long, H. Ou, J. M. Kuo, K. K. Chin, IEEE Trans. Electron Devices, **46(**5), 396 (1999).
[12] H. Jiang, S. Shao, W. Cai, P. Zhang, Journal of Computational Physics, **227(**13), 6553 (2008).
[13] B. Syamal, C. K. Sarkar, P. Dutta, N. Mohankumar, International Conference on Microelectronics, pp. 44, 2010.
[14] Jean-Pierre Colinge, "FinFETs and Other Multi-Gate Transistors", Springer, 2007.
[15] Sentaurus Device User Guide, Synopsys Inc.,Version D-2010.03.

* Corresponding author: theodorechandra@gmail.com
theodore@tce.edu